Supplementary Information

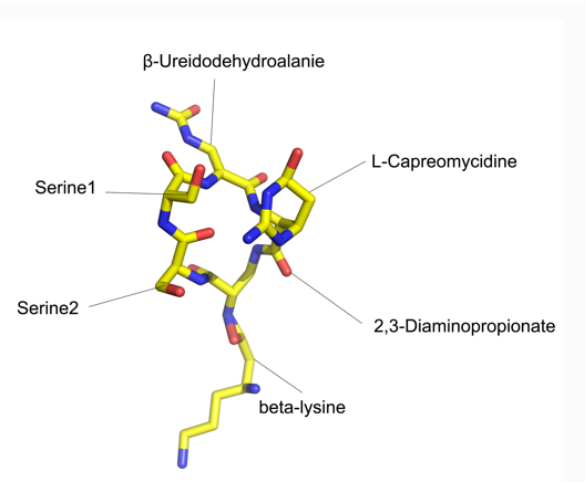

Figure S1. Structure of Viomycin. Viomycin is a cyclic pentapeptide containing β-ureidodehydroalanine , L-capreomycidine, two serines and a 2,3-diaminopropionate linked to a β-lysine tail.

Materials and Methods

Preparation of Ribosome-tRNA-mRNA-Viomycin Complex for Cryo-EM

Tight-couple 70S ribosomes were prepared from *E. coli* MRE600 as described (1) . $tRNA^{fMet}$ was overexpressed and purified as described in reference (2). Defined mRNA MO-27 was synthesized by Integrated DNA Technologies. Viomycin was purchased from Sigma Aldrich. The ribosome-tRNA-mRNA-viomycin complex was formed by first incubating 40 pmol 70S ribosomes, 80 pmol mRNA M0-27 (5'-GGCAAGGAGGUUUAAAUGUAAAAAAAA), 80 pmol deacylated $tRNA^{fMet}$ in buffer A (20 mM Tris·HCl pH 7.0, 100 mM NH_4Cl, 10.5 mM $MgCl_2$, 0.5 mM EDTA), followed by addition of viomycin to a concentration of 0.5 mM and incubating for 20 min at 37 ºC.

Cryo-EM Sample Preparation

Quantifoil holey carbon grids were washed first in ethyl acetate (Merck) and glow-discharged for 90 seconds using a PELCO EasiGlow Discharge Cleaning System. Aliquots of 2.5 µl of 70S ribosome-tRNA-mRNA-viomycin complex at a concentration of ~50 nM were subsequently incubated on grids which had previously been deposited with a home-made carbon film, followed by immediate flash freezing in liquid ethane using an FEI Vitrobot. Cryo-EM data were acquired using a Titan Krios cryo-transmission electron microscope equipped with a Gatan K2 Summit direct electron detector at 300 KV. Micrographs were collected at a magnification of 75,000X (effective pixel size = 1.017 Å at the object scale) with defocus ranging from -1.5 to -2.5 µm. For

each micrograph stack, 24 frames were collected, with a total dose of 17 electrons per pixel.

Cryo-EM Data Processing

Motion correction of the micrograph was performed using MOTIONCORR (3), followed by estimation of CTF parameters using CTFFIND3 (4). 13,000 particles were picked using semi-automated particle picking with EMAN2. Further image processing, including 2D classification, 3D classification, and high-resolution refinement was performed in RELION 2.0 (5). Reference-free 2D class averaging was used to identify bad particles, which were discarded during initial 3D reconstruction and later refinements.

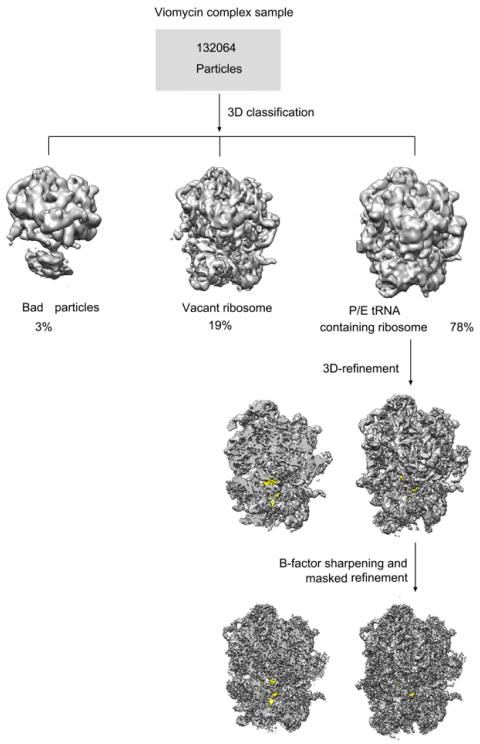

Figure S2. Flow-chart for cryo-EM data processing and structure determination. The 3D classification (Relion) resulted in three classes of particles. The P/E tRNA-containing ones were used for further 3D refinement, B factor sharpening and masked refinement. Viomycin molecules are shown in yellow at the bottom.

Table S1. Statistics of Cryo-EM Structural Determination and Model Refinement

70S Ribosome-tRNA-mRNA-Viomycin Complex
Data collection

Electron microscope	Titan Krios
Voltage (kV)	300
Electron detector	Falcon II camera
Electron dose (e−/Å2)	~20
Pixel size (Å)	1.08
Defocus range (μm)	1.5–2.5
Reconstruction and model refinement	
Particles for final refinement	84,240
Resolution of unmasked map (Å)	4.1
Resolution of masked map (Å)	3.8
Map-sharpening *B* factor ($Å^2$)	–30
R factor	0.33
Fourier shell correlation	0.71
Model composition	
Peptide chains	51
Residues	
RNA chains	3
RNA nucleotides	4554
R.m.s. deviation	
Bond length (Å)	0.005
Bond angle (°)	1.2
Ramachandran plot	
Favored (%)	88.80
Outliers (%)	2.47
Validation (protein)	
MolProbity score	2.01 (99th percentile)
Clashscore	1.74 (100th percentile)
Good rotamers (%)	85.91
Validation (RNA)	
Correct sugar puckers (%)	98.76
Good backbone conformations (%)	73.85

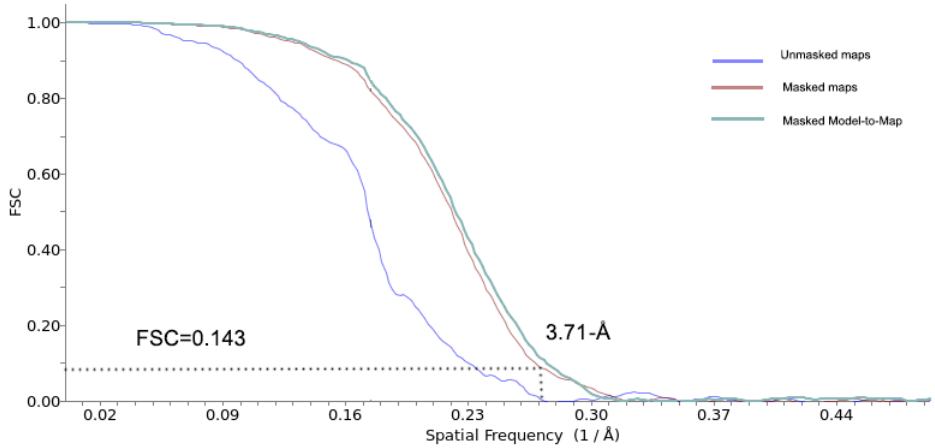

Fig S3. Fourier shell correlation curves, showing resolution of 3.71Å at FSC = 0.143.

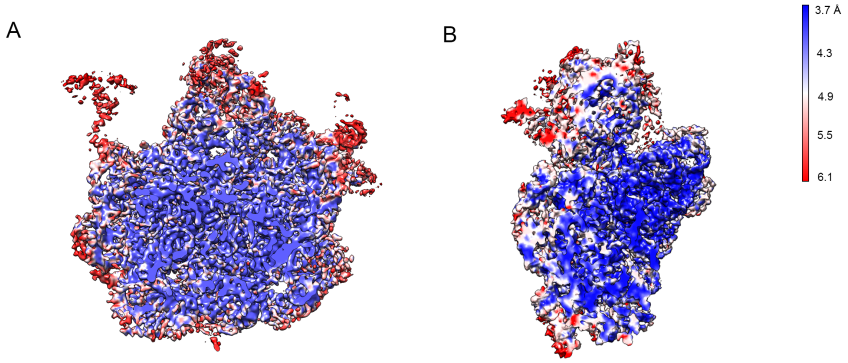

Fig. S4. Local resolution for the cryo-EM map, viewed from the subunit interface for (A) 50S subunit; (B) 30S subunit.

Crystallization, Data Collection, Model Building and Refinement

The viomycin-RF3-ribosome complex containing a 27-nucleotide mRNA and $tRNA^{Met}$ was prepared as described previously (6). Crystals were grown via vapor diffusion in 96-well plates by adding 1.5 µl of reservoir solution (100 mM Tris·HCl (pH 7.0), 25–35 mM KCl, 6.1% PEG20K, 1% glycerol, 50 mM sucrose), to 1 µl of complex. Crystals were grown at 23ºC by sitting drop vapor diffusion. Crystals grew in 5 days to the size of up to 300 X 150 X 50 µm. and were stabilized in a cryo-protection buffer containing 50 mM KOAc (pH 5.0), 6.5% PEG20K, 20% PEG400, 50 mM sucrose, 1% glycerol, 0.5 mM GDPNP, and 0.5 mM viomycin, followed by flash freezing in liquid nitrogen. Crystal screening and data collection were carried out at BL17U at the Advanced Photon Source (APS), the Advanced Light Source (ALS) and the Shanghai Synchrotron Radiation Facility (SSRF) using 0.2º oscillations. Diffraction data from one crystal were integrated,

merged and scaled in XDS (7). The crystal structure was solved by molecular replacement in Phaser (8) using an all-atom model of the ribosome-RF3-GDPNP structure at 3.7-Å for initial search. The initial solution was refined by 2-rigid-body refinement followed by 300-rigid-body refinement as described previously (9). An unbiased simulated-annealing omit map was subsequently calculated with Phenix (10) by using a starting temperature of 3000º K. The resulting omit map revealed five viomycin molecules, four of which were bound at the 30S-50S subunit interface. Viomycin models were manually fitted into the omit map using Coot (11) followed by B factor minimization and TLS refinement in CNS (12) and Phenix (10).

Table S2. Crystallographic data collection and structure refinement

Data collection	70S-ribosome-RF3-GDPNP-mRNA-tRNA complex (from one crystal)
Space group	$P2_12_12_1$
Unit cell dimensions:	
a, b, c (Å)	a = 257.6 b = 312.9 c = 328.6
α, β, γ (°)	α = β = γ= 90º
Resolution (Å)	50-3.0 (3.2-3.0)
Overall Mosaicity	0.25
R_{sym}	33.7 (81.9)
I/σ(I)	5.61 (0.8)
Completeness	98.1% (90%)
Redundancy	4.1(2.3)
Refinement	
Resolution (Å)	3.0-50
No. unique reflections	515,115
R_{work}/R_{free}	23.3/25.1
R.m.s. deviations:	
Bond lengths (Å)	0.006
Bond angles (°)	1.256

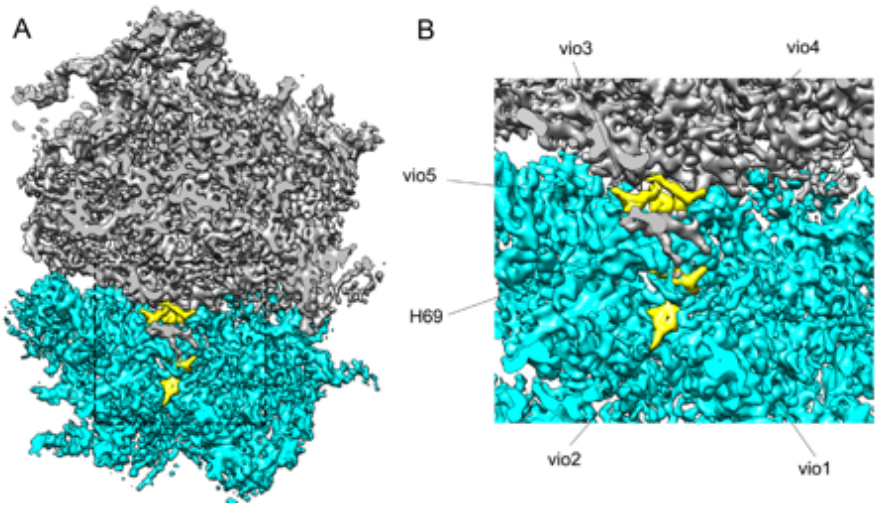

Figure S5. Cryo-EM density for viomycin molecules. (A) Overall view, showing 30S (cyan) and 50S (grey) subunits. **(B)** Expanded view showing cryo-EM density for all five viomycins (yellow).

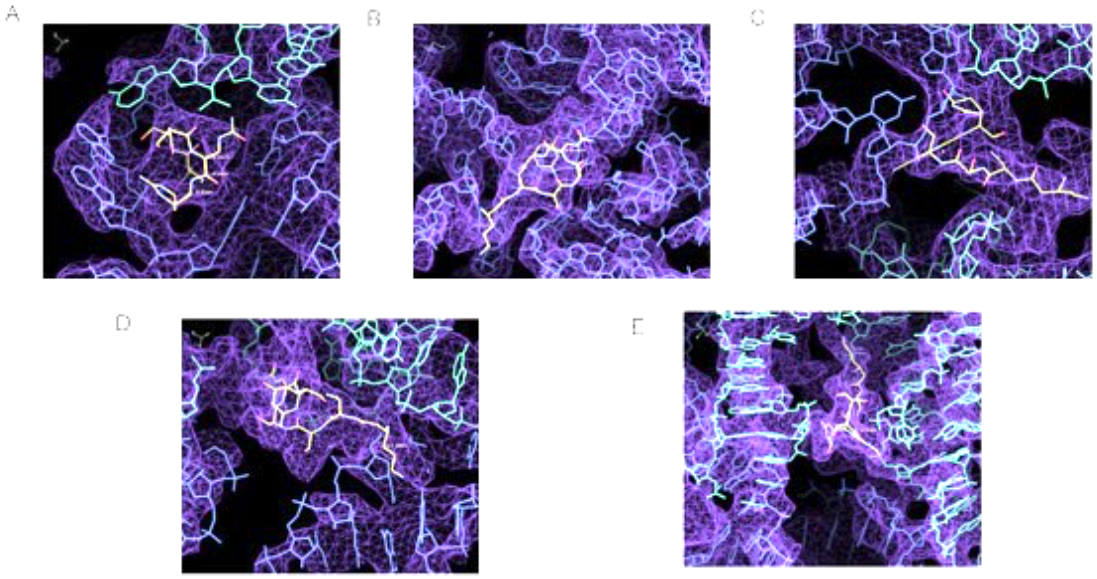

Fig. S6. Local cryo-EM density for the five bound viomycins: (A) Vio1, (B) Vio2, (C) Vio3, (D) Vio4, (E) Vio5.

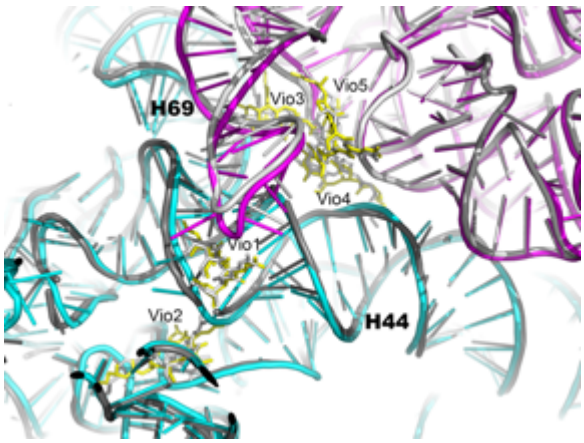

Fig. S7. Superimposition of the 5 viomycin molecules from the x-ray structure (yellow) and cryo-EM structure (white). Corresponding superimposed structural models for the 16S rRNA and 23S rRNA are shown for the x-ray structure (cyan and grey) and cryo-EM structure (black and white).

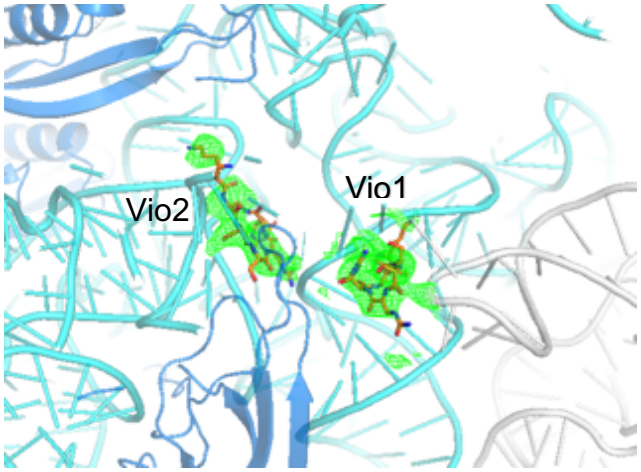

Figure S8. X-ray electron Density for Vio1 and Vio2. Simulated-annealing omit F_o-F_c electron density contoured at 2.5σ (green) is shown for Vio1 and Vio2, in the context of 16S rRNA (cyan), 30S ribosomal proteins (blue) and 23S rRNA (grey).

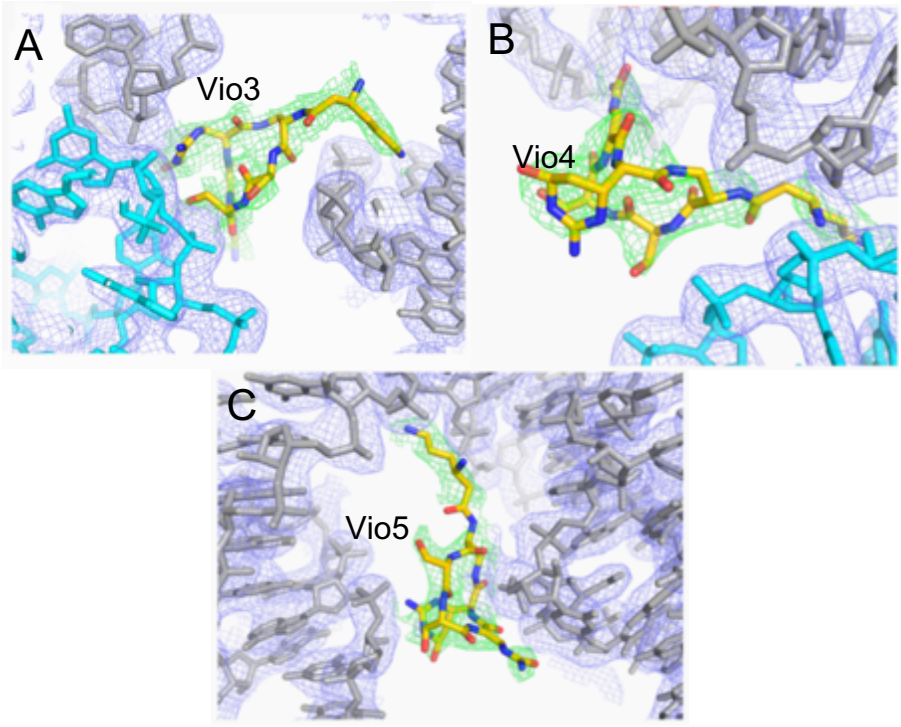

Figure S9. X-ray electron Density for Vio3, Vio4 and Vio5. Simulated-annealing omit F_o-F_c electron density contoured at 2.5σ (green) is shown for **(A)** Vio3 **(B)** Vio4 and **(C)** Vio5 in the context of 16S rRNA (cyan) and 23S rRNA (grey). $2F_o$-F_c electron density for ribosomal RNA (blue) is contoured at 1.5σ.

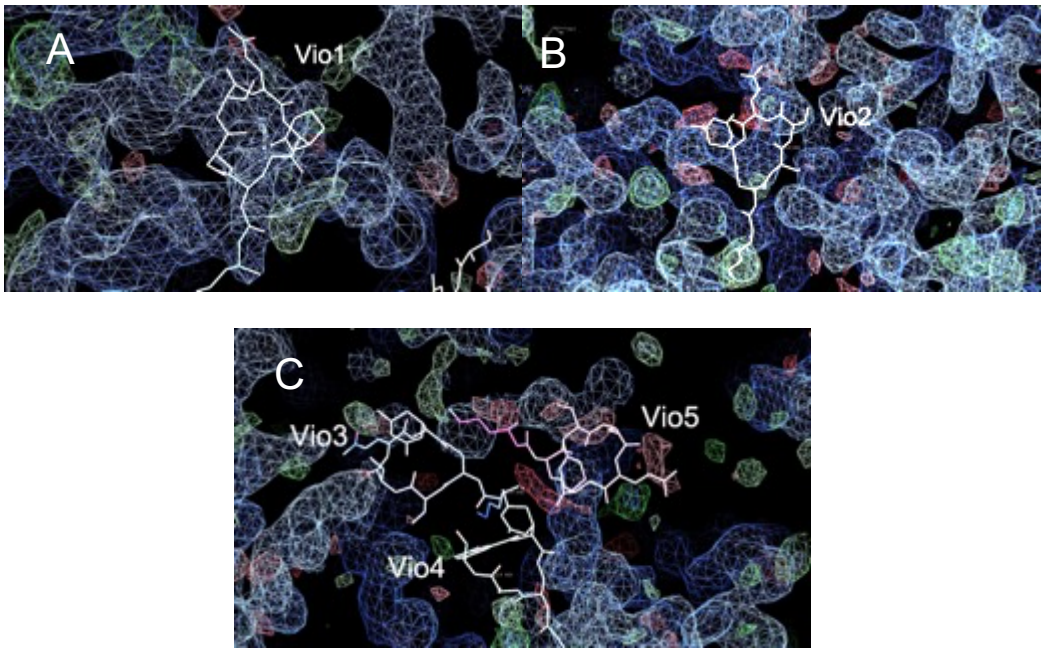

Fig. S10. Absence of Vio3, Vio4 and Vio5 in the Classical-State Viomycin complex. The five viomycin molecules from this work are superimposed on the corresponding positions in x-ray electron density maps from the classical-state viomycin-ribosome complex (13). The maps shown are $2F_o$-F_c contoured at 1.5σ (blue) and F_o-F_c contoured at +2.5σ (green) and -2.5σ (red). **(A)** Clear $2F_o$-F_c density is visible for Vio1. **(B)** Some $2F_o$-F_c density corresponding Vio2 may be present. **(C)** $2F_o$-F_c density is clearly absent for Vio3, Vio4 and Vio5. No positive or negative F_o-F_c difference density is apparent for any of the viomycins.

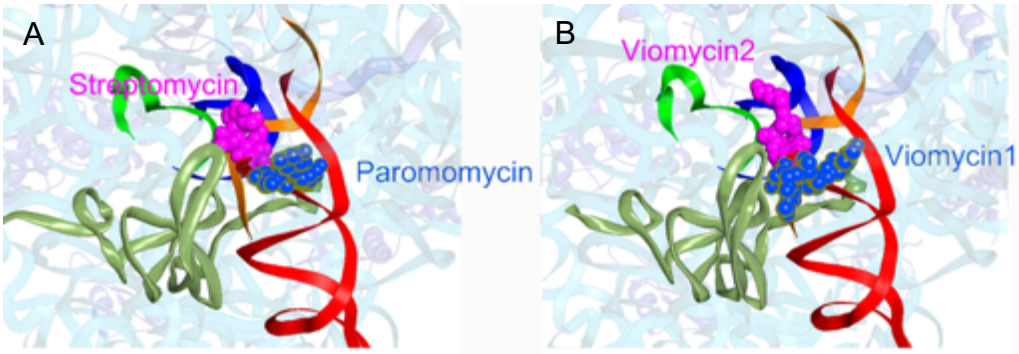

Figure S11. Overlap Between the Binding Sites of Streptomycin and Vio2. (A) Positions of **(A)** streptomycin and paromomycin (14) and **(B)** Vio1 and Vio2 around the decoding site of the 30S ribosomal subunit.

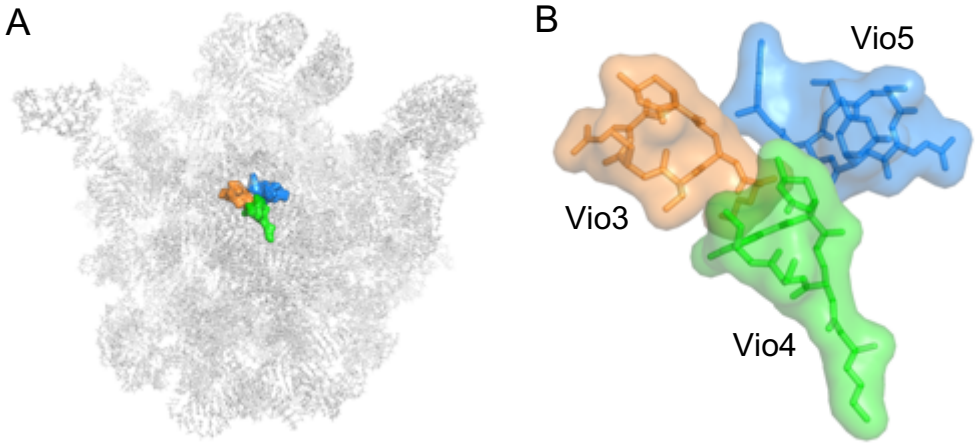

Fig. S12. Clustering of Vio3, Vio4 and Vio5. (A) Position of the Vio3-Vio4-Vio5 cluster relative to 23S rRNA. **(B)** Contact between Vio3, Vio4 and Vio5, shown in transparent surface rendering.

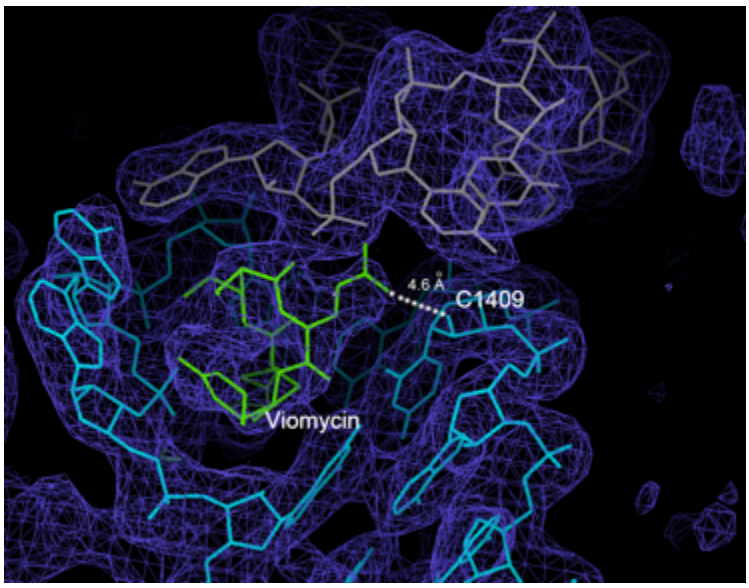

Fig. S13. Close Approach of Vio1 to Ribose 1409 of 16S rRNA. Methylation of the 2'-OH of ribose 1409 confers sensitivity of *B. smegmatis* to capreomycin and viomycin (15, 16). It is possible that this methylation creates contact with Vio1 (green), which is separated from C1409 by 4.6Å in the non-methylated *T. thermophilus* structure (above). 16S rRNA is shown in cyan, 23S rRNA in grey. $2F_o$-F_c electron density, contoured at 1.5σ is shown in blue.

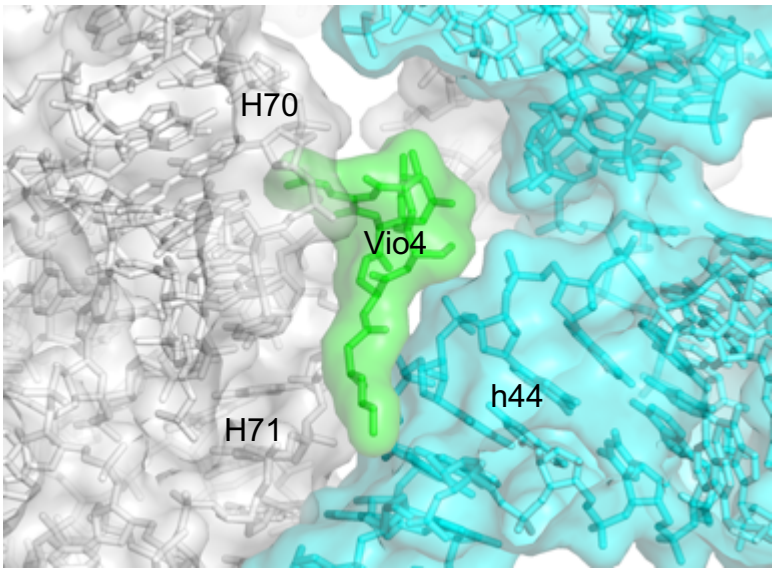

Figure S14. Binding of Vio4 at Intersubunit Bridge B3. Vio4 (green) binds at bridge B3, which coincides with the axis of 30S rotation. Vio4 contacts H70 and H71 of 23S rRNA (grey) on one side and h44 of 16S rRNA (cyan) on the other side.

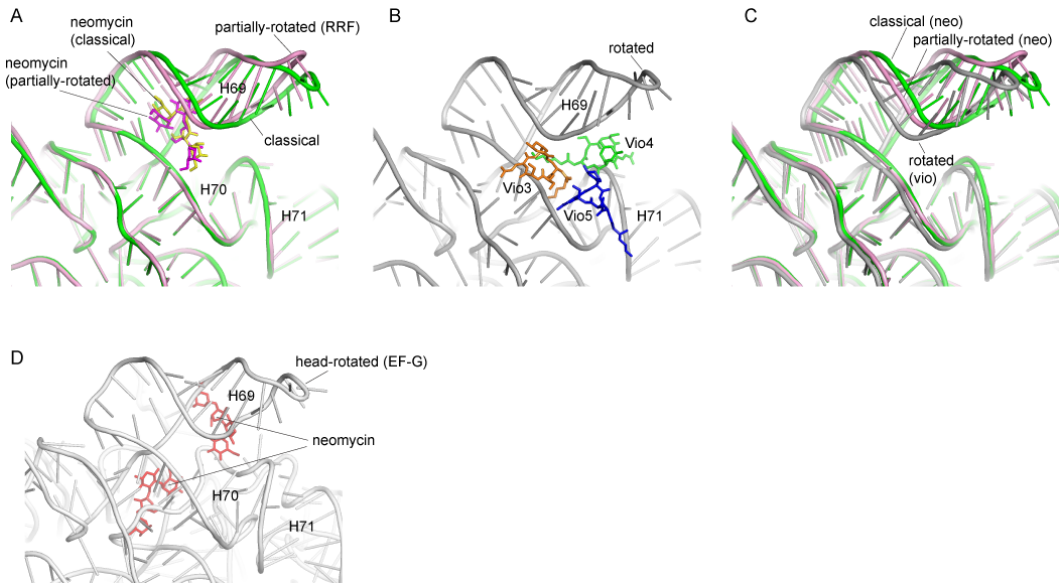

Fig S15. Viomycin and neomycin bind to different sites on H69 and have different effects on the conformation of H69. (A) Neomycin (cyan) bound to a classical-state ribosome (green) containing P-tRNA (17) is overlaid with neomycin (magenta) bound to a partially-rotated complex (pink) containing ribosome recycling factor (RRF) and tRNA bound in an intermediate state between P/P classical and P/E hybrid (17). **(B)** Vio3 (orange), Vio4 (green) and Vio 5 (blue) bound to a fully-rotated ribosome (grey) (this work). **(C)** Comparison of the positions of 23S rRNA H69 in the neomycin-bound classical-state (green) and partially-rotated (pink) ribosomes (17), with that of the viomycin-bound fully-rotated ribosome (this work) (grey). **(D)** In the chimeric hybrid-state ribosome complex containing EF-G and two tRNAs (9), the two neomycins (red) bind to completely different binding sites from those in the structures shown in panel (A).

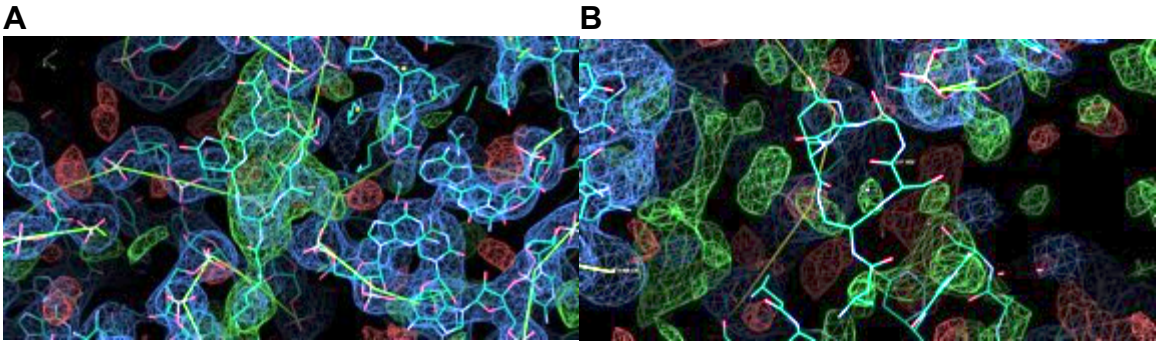

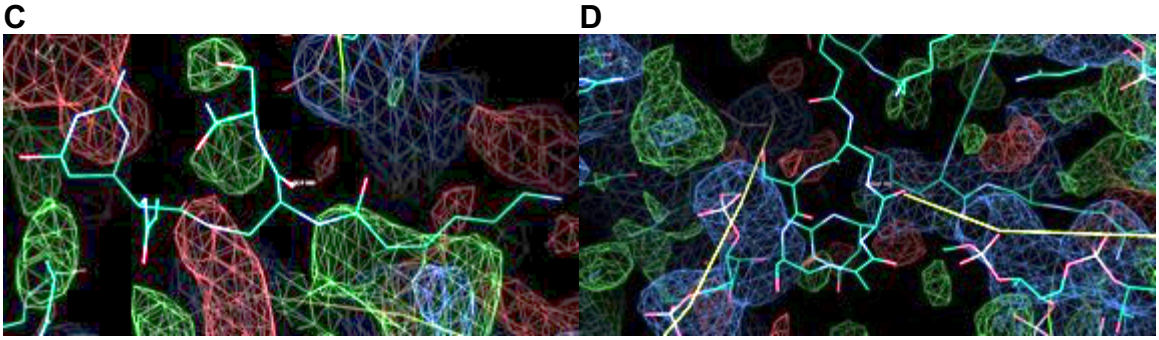

Fig. S16. Electron Density at the Positions of Vio2, Vio3, Vio4 and Vio5 for a complex containing EF-G bound to vacant, rotated ribosomes (18). (A) Vio2; **(B)** Vio3; **(C)** Vio4; **(D)** Vio5. Electron density is present for Vio2, but not Vio3, Vio4 or Vio5.

References

1. Lancaster L, Kiel M, Kaji A, & Noller H (2002) Orientation of Ribosome Recycling Factor in the Ribosome from Directed Hydroxyl Radical Probing. *Cell* 111:129-140.
2. Borel F, Hartlein M, & Leberman R (1993) In vivo overexpression and purification of Escherichia coli tRNA(ser). *FEBS Lett* 324(2):162-166.
3. Li X*, et al.* (2013) Electron counting and beam-induced motion correction enable near-atomic-resolution single-particle cryo-EM. *Nat Methods* 10(6):584-590.
4. Mindell JA & Grigorieff N (2003) Accurate determination of local defocus and specimen tilt in electron microscopy. *J Struct Biol* 142(3):334-347.
5. Scheres SH (2012) RELION: implementation of a Bayesian approach to cryo-EM structure determination. *J Struct Biol* 180(3):519-530.
6. Zhou J, Lancaster L, Trakhanov S, & Noller HF (2011) Crystal structure of release factor RF3 trapped in the GTP state on a rotated conformation of the ribosome. *RNA* 18(2):230-240.
7. Kabsch W (1993) Automatic processing of rotation diffraction data from crystals of initially unknown symmetry and cell constants. . *J. Appl. Cryst.* 26:795-800.
8. McCoy AJ*, et al.* (2007) Phaser crystallographic software. *J Appl Crystallogr* 40(Pt 4):658-674.
9. Zhou J, Lancaster L, Donohue JP, & Noller HF (2014) How the ribosome hands the A-site tRNA to the P site during EF-G-catalyzed translocation. *Science* 345(6201):1188-1191.
10. Adams PD*, et al.* (2010) PHENIX: a comprehensive Python-based system for macromolecular structure solution. *Acta Crystallogr D Biol Crystallogr* 66(Pt 2):213-221.
11. Emsley P & Cowtan K (2004) Coot: model-building tools for molecular graphics. *Acta Crystallogr D Biol Crystallogr* 60(Pt 12 Pt 1):2126-2132.

12. Brunger AT*, et al.* (1998) Crystallography & NMR system: A new software suite for macromolecular structure determination. *Acta Crystallogr D Biol Crystallogr* 54(Pt 5):905-921.
13. Stanley RE, Blaha G, Grodzicki RL, Strickler MD, & Steitz TA (2010) The structures of the anti-tuberculosis antibiotics viomycin and capreomycin bound to the 70S ribosome. *Nat Struct Mol Biol* 17(3):289-293.
14. Carter AP*, et al.* (2000) Functional insights from the structure of the 30S ribosomal subunit and its interactions with antibiotics. *Nature* 407(6802):340-348.
15. Johansen SK, Maus CE, Plikaytis BB, & Douthwaite S (2006) Capreomycin binds across the ribosomal subunit interface using tlyA-encoded 2'-O-methylations in 16S and 23S rRNAs. *Mol Cell* 23(2):173-182.
16. Maus CE, Plikaytis BB, & Shinnick TM (2005) Mutation of tlyA confers capreomycin resistance in Mycobacterium tuberculosis. *Antimicrob Agents Chemother* 49(2):571-577.
17. Wang L*, et al.* (2012) Allosteric control of the ribosome by small-molecule antibiotics. *Nat Struct Mol Biol* 19(9):957-963.
18. Pulk A & Cate JH (2013) Control of ribosomal subunit rotation by elongation factor G. *Science* 340(6140):1235970.